Supporting Information

de Beco et al. 10.1073/pnas.0811253106

SI Text

FRAP Data Analysis. A home-made Matlab program was developed for FRAP data analysis to take into account:

1. The observational photobleaching. Because the total intensity on a stack at any given time after bleach is expected to reflect a constant total number of fluorescent molecules in each cell, that intensity must be normalized to compensate for the observational photobleaching, i.e., the unwanted photobleaching during the observation. This correction was made by keeping the distribution of pixel intensity throughout any given stack equal the corresponding distribution assessed just after photobleaching. This approach avoids a suppression of a "background noise," which is difficult to appreciate and varies in time due to camera artefacts.
2. The movements of the junctions. Junctions were manually drawn the computer mouse as broken lines, and smoothed by "spline" interpolation. Movements were estimated by superimposing the first profile with the last image. If motion was detected during the observation period, a serie of intermediate profiles could be drawn by the user, at regularly spaced intermediate time points chosen by the user as a function of movement amplitude. The remaining profiles were approximated by linear interpolation.

In some cases, this routine was not adequate to correct for the motion of the junction. Typically, the program works correctly for motions perpendicular to the junction, whereas lateral shifts of the junction or shrink/expansion may not be well corrected for. Therefore, a systematic visual inspection of the kymographs (*cf.* Fig. 2*B*) was performed, allowing to detect lateral movements of the photobleaching area. In these cases of poorly corrected movements (representing up to 30–50% of cases for long observation times of 20 min), the data were disregarded.

FRAP Data Interpretation. The general frame for interpreting FRAP data are based on considering two elementary processes (membrane diffusion, immobile or reaction-limited exchange) or a combination of them.

Diffusion. Simple diffusion was approximated as 1D diffusion along the junction line. Indeed, two-photon photobleaching was restricted in height, but the subsequent collection of images was done through 1-photon videomicroscopy, with image stacks that were then projected onto one image. Note that deconvolution was not used for the quantitative analyses, because it is practically not a reliably linear procedure.

Reaction-Limited Exchange. Our basic underlying assumption is that the overall transport of cadherin molecules through their different localizations and chemical states is made of steady-state processes. In other words, the fluxes between all states are constantly balanced. A direct consequence is that the net flux off the membrane by endocytosis is balanced by exocytosis. These two fluxes are coupled in a way that is not known, but we assumed that a block of the endocytosis rapidly leads a block of the exocytosis. This assumption reflects accurately our observations. As in our previous study (1), we assumed that diffusion inside the plasma membrane as well as inside the cytosol are fast enough compared to endocytosis, so that diffusive pools are practically uniform. In addition, if the cell does regulate endocytosis efficiency, one can assume for the sake of simplicity, that it obeys a first order process. Relaxation kinetics is then exponential, with a time constant that we assumed to be in space and time.

Combination of two independent pools, with diffusive and "exchanging" behaviors (corresponding to the case treated in the main text). In the case where two independent pools coexisted with no exchange between them, one diffusing at membrane and one undergoing endocytosis/exocytosis, their relative amount could be calculated by assessing how much the fluorescence profile broadens (Fig. 1), provided the membrane diffusion coefficient and exchange time τ_c are known.

The theoretical study was performed for 1D and 2D diffusion, and the 1D case only is presented in the manuscript. An example is shown in Fig. S1*A*, in the case of a 50–50% combination, with a fixed diffusion time τ_d and a variable residence time τ_c: note that for $\tau_c \geq 100\tau_d$, which is typically the case here, the broadening due to diffusion becomes less visible (albeit still detectable). Indeed diffusion-induced broadening occurs at times shorter than the first order relaxation time, so that at these times the fit of σ is dominated by the "exchange" pool that has not yet relaxed.

As mentionned in the results section, if one assumes the membrane diffusion coefficient equals 5×10^{-2} $\mu m^2 \cdot s^{-1}$ and given the τ_c values extracted from FRAP experiments (240 s or 50 s), the broadening of fluorescence profiles indicates that the pool of freely diffusive E-cadherins does not exceed 5% (resp. 10%) in MCF7 (resp. MDCK) cell junctions.

"Semiindependent" combination. A more general scenario (Fig. S1*B*) is to couple three states (membrane diffusion, immobile at the membrane, cytosolic diffusion), with exchange rates between them. Indeed, from a biological viewpoint, the pools depicted in the previous paragraphs are likely to exchange molecules, and are therefore problably not independent. A more realistic situation is that molecules are exchanged between free diffusion at the membrane and engagement in adhesive bonds. Indeed, we observed that the diffusive fraction virtually disappears when endocytosis is blocked. As described above, the relative size of the free membrane diffusing (Q_D) and the membrane engaged/endocytosed pools (Q_I) were assessed from the broadening of fluorescence profiles. Practically: $Q_D k_{eng} = Q_i (K_{endo} + k_{dis})$. With $Q_D/Q_i \leq 5\%$ (in MDCK cells), and $k_{endo} = 0.0043\ s^{-1}$, one obtains: $k_{eng}/k_{dis} = Q_i/Q_D)k_{endo}k_{dis} + 1) \geq 20$ (i.e., $k_{eng} > 20k_{dis}$).

This means that the off-rate of cadherins from the engaged state is negligible compared to the on rate, and that the fate of engaged cadherins is not to revert to the membrane diffusion state, but predominantly to undergo endocytosis. In other words, cadherin engagement from the free diffusion state is practically an irreversible process.

Effective diffusive pool undergoing a reaction-limited exchange (not treated in the main text). If one considers the possibility of fast exchange of molecules between the membrane diffusive and the immobile (engaged) pool (see Fig. 1*B*), the previous approximation of semiindependent pools no longer holds. Our approach was here to consider a single membrane pool with a smaller "effective" diffusion coefficient D_{eff} (2) (Fig. S1*C*): indeed successions of diffusion/trapping phases observed in Single Particle Tracking (SPT) (3) have been previously reported to behave as a slower effective diffusion in FRAP experiments (4). This approximation holds if diffusive and trapping phase are alternated several times during the residence of the molecule at the membrane (2).

In that situation where an effective membrane diffusion is combined with endocytosis one can write two coupled diffusion

equation obeyed by the concentration at the plasma membrane and in the cytosol. For dimensionality reason, the surface concentration is rescaled by the constant (1/R), using a typical cell size R. Let's define the volume concentration f of cytosolic molecules, and the rescaled surface concentration c of membrane fluorescent molecules:

$$\begin{cases} \dfrac{\partial c}{\partial t} = D_{\text{eff}}\nabla^2 c - k_{\text{endo}}c + k_{\text{exo}}f \\ \dfrac{\partial f}{\partial t} = D_{\text{ves}}\nabla^2 f - k_{\text{exo}}f + k_{\text{endo}}c \end{cases} \quad [1]$$

where D_{eff} is the effective diffusion coefficient at the plasma membrane and D_{eff} the vesicular diffusion coefficient in the cytoplasm.

Under the assumption of a reaction-limited process (2), i.e., if vesicular diffusion time over the cell size is short compared to the exocytosis time and to the timescale of FRAP experiments, the cytosolic concentration $f = f_{eq}$ is constant and $\dfrac{f_{eq}}{c_0} = \dfrac{k_{\text{endo}}}{k_{\text{exo}}}$. ($c_0$ steady-state concentration),

Eq. **1** then becomes:

$$\frac{dc}{dt} = D_{\text{eff}}\nabla^2 c - k_{\text{endo}}c + k_{\text{exo}}f_{eq} \quad [2]$$

with $c^* = c - c_0$, Eq. **2** becomes:

$$\frac{dc^*}{dt} = D_{\text{eff}}\nabla^2 c^* - k_{\text{endo}}c^* \quad [3]$$

With the initial conditions of a Gaussian concentration profile of width a, a solution of Eq. **3** is:

$$c^*(x,t) = \frac{a}{2\sqrt{\pi}}\int_{-\infty}^{+\infty} \exp(-\zeta^2 a^2/4 - i\zeta x - (k_{\text{endo}} + D_{\text{eff}}\zeta^2)t)d\zeta$$

$$= \frac{a}{2\sqrt{\pi}}\exp(k_{\text{endo}}t)\int_{-\infty}^{+\infty}\exp(-\zeta^2(a^2 + 4D_{\text{eff}}t)/4 - i\zeta x)d\zeta. \quad [4]$$

The solution is a Gaussian profile, and its width depends on the membrane diffusion process (resulting $\sigma = \sqrt{a^2 + 4D_{\text{eff}}t}$), but not on the exchange process (characterized by k_{endo}) which influences only the depth.

It follows that the spatial broadening in time only depends on the effective membrane diffusion coefficient D_{eff} and not on the kinetics of endo- exocytosis (Fig. S1*D*).

The above method was used to set an upper bound to the effective diffusion coefficient in MDCK and MCF7 junctions in this hypothesis of fast membrane exchanges. From error bars of the estimates of the width of Gaussian fits (Figs. 2 *D* and 4*C*), an estimate of the maximal effective diffusion coefficient was 2×10^{-4} μm^2·s^{-1} for both MDCK and MCF7 cells. The fact that this value is very small compared to the diffusion coefficients previously measured for cadherins (10^{-3} to 5×10^{-2} μm^2·s^{-1}) (3), is again consistant with the notion that diffusion of free cadherins is not the dominant process of relaxation at short times (Fig. 2*E Inset*). As a conclusion, the hypothesis of fast membrane exchanges was not further considered.

***Z* Distribution of E-Cadherin Labeling.** In *adherens* junctions of MDCK cells, E-cadherin-GFP fluorescence is seen as a vertical stripe of 2.5 μm height, with roughly uniform intensity (see Fig. S2). Our FRAP experiments only targeted this band, and not a putative more diffuse form in the junction. In our experiments, the z resolution (z point spread function) of the two-photon microscope is 1.8 μm (NA = 1.25), and that is similar to the vertical extension of E-cadherin localization. Therefore, our experiments reveal the behavior of E-cadherins spatially averaged over the region where is is expressed. We checked that FRAP experiments gave the same results when performed at the bottom or at the top or in the middle of the expression stripe.

Image Processing for Colocalization Data. We show here an original image (Fig. S3*a*) and its processing (Fig. S3), for FM4–64 (red)/E-cadherin-GFP (green) containing vesicles. This is a typical image from which newly formed vesicles were counted (25 yellow and 136 green vesicles were counted in step 3c; for more visibility despite image reduction, Fig. S3*d* is represented in the main manuscript in Fig. 3).

Control for the Effect of Dynasore. The first papers on dynasore or MiTMAB reagents (5, 6) established that, in a number of cell types, the morphology was not perturbed with concentrations and incubation time as used here. We further controlled this point, by checking that the morphology of adherens junctions was preserved after dynasore treatment, with similar patterns of ZO-1 and E-cadherin immunolabeling in untreated and treated cells (Fig. S4).

Method: After fixation in methanol at −20 °C for 15 min, the following primary antibodies were used: rat monoclonal against E-cadherin (ECCD-2, Axxora) and rabbit polyclonal against ZO-1 (Zymed), and as secondary antibodies anti-rat alexa 350 and anti-rabbit alexa 555 (Invitrogen). Cells were mounted in mounting medium (Vectorlabs) and viewed by epifluorescence with a Leica DM6000B microscope. Images stacks were deconvolved using Metamorph (Universal Imaging).

Formation of New E-Cadherin Containing Vesicles in Wild-Type MDCK. We performed experiments of vesicular staining on MDCK cells to rule out the possibility that the fast endocytosis of E-cadherin-GFP could be an artifactual behavior due to the GFP moiety or cadherin overexpression. Table S1 shows that E-cadherin containing vesicles in wild-type MDCK cells form at the same rate as E-cadherin-GFP containing vesicles in transfected MDCK cells (Fig. S5, and "colocalization" column in Table S1). In addition, those rates of endocytosis are blocked in both cases by dynasore (Fig. S5, Table 1 and Table S1) and MiTMAB (data not shown). In addition, general endocytosis occurs at the same rate in both cells types and is blocked by both inhibitors, as demonstrated by counting FM4–64 positive vesicles. When the total number of cadherin-containing vesicles is assessed, larger numbers are found for wild type cells. This may be due to technical reasons: (*i*) antibody-mediated detection of cadherin is much more efficient than with GFP fluorescence, and (*ii*) the required tradeoff between fixation and permeabilization requirements for the simultaneous visualization of FM4–64 and E-cadherin with wild-type cells leads to a procedure that make it difficult to compare with transfected cells. However, the important result is that the percentage of newly formed E-cadherin vesicles is unchanged in wild-type vs. transfected cell lines (colocalization).

Method: After treatment by control medium or dynasore 60 μM for 15 min, WT MDCK cells were incubated with FM4–64FX (Invitrogen) 5 μg/ml for various times, rinsed three times in cold PBS, fixed with 4% paraformaldehyde/0.25% glutaraldehyde in PBS for 10 min at 4 °C and permeabilized with 0.05% saponin. Rat monoclonal against E-cadherin (ECCD-2, Axxora) and anti-rat alexa 488 (Invitrogen) were used respectively as primary and secondary antibodies. Cells were mounted in

mounting medium (Immu-mount, Thermo Scientific) and viewed by confocal microscopy with a Leica TCS SP2.

Western Blots for the Comparison of Wild-Type and Transfected Cell Lines. To further address the effect of E-cadherin-GFP expression in transfected cell lines, we quantified the total amount of E-cadherin in Western blots done on MDCK vs. MDCK-E-cadherin-GFP, and on MCF7 vs. MCF7-E-cadherin-GFP. We show that the total amounts of E-cadherin in wild-type and transfected cell lines are similar (Fig. S6). This further indicates that the dynamics of E-cadherin is not likely to be affected by the GFP tag (see Table S2).

Method: Confluent cells were directly resuspended in loading buffer (60 mM trisHCl, 2% SDS, 10% glycerol, 10% β-mercaptoethanol) and DNA was removed by centrifugation. After PAGE migration and transfer, the PVDF membrane was incubated with primary antibodies directed against E-cadherin (from rat ECCD-2, Axxora) and actin (A4700, Sigma). The secondary antibodies were an anti-rat and an anti-mouse IgG conjugated to peroxidase revealed by the SuperSignal West Pico kit (Pierce).

In Dissociating MDCK Junctions, Redistribution Mainly Involves Membrane Diffusion. We compared E-cadherin dynamics in mature and non-mature *adherens* junctions. Because the cadherin signal was too weak to perform a quantitative study before the onset of contacts, we studied junctions during their dissociation instead. Mature junctions were first partially dissociated with EDTA, calcium was then restored to an intermediate concentration (100 μM) before the dissociation was complete, and endocytosis was blocked with dynasore. Cells were in most cases still in contact, but had a weaker E-cadherin GFP signal (Fig. S7*a*), probably reflecting a reduced number of molecular bonds.

FRAP experiments on nearly dissociated contacts (Fig. S7*a*, red ellipse), revealed a fast relaxation despite inhibition of endocytosis by dynasore. Moreover, the photobleached area widened with time (Fig. S7 *b* and *c*), indicating a diffusive behavior. More precisely, the square width σ^2 of the Gaussian profile increased linearly with time (Fig. S7*c*), as expected from a diffusion process, and a diffusion coefficient $D = 0.0025$ $\mu m^2 \cdot s^{-1}$ was found (Fig. S3*d*) (7). This value is unlikely to correspond to free membrane diffusion because it is one order of magnitude lower than values reported in the litterature for E-cadherin free membrane diffusion (3, 8–10). In partially dissociated junctions instead, the diffusion coefficient measured (Fig. S7*d*) might correspond to an "effective" diffusion coefficient, indicating free diffusion with fast exchange with the remaining engaged junctions (Fig. S7*e*), without involvement of the endocytic pathway (because the signal is not blocked by dynasore). Such behavior has previously been observed for E-cadherin in some experimental situations without engagement (3, 4), and these repeated observations form the basis of the current view that local cadherin concentration can be regulated independently of endocytosis by disengagement, diffusion and reengagement. We have shown in this study that this diffusion-based behavior is indeed observable in dissociating junctions but not in mature ones.

In dissociating junctions, in the absence of dynasore, we observed a combined behavior, that very likely includes a diffusive component (widening of σ^2) coupled to an exchange one (the recovery curve is not fit by diffusion only). However, the similar time scales for the two processes make the analysis difficult in as to clearly separate these two contributions.

Note that the present experiments on junctions during dissociation also allow to exclude the possibility of undesirable side-effects of dynasore such as (*i*) a global freezing of membrane protein diffusion, or, more subtly, (*ii*) an inhibition of cadherin lateral detachment from *cis*/*trans* contacts. Under our experimental conditions, despite the presence of dynasore, diffusion was still observed (slow in dissociating contacts and faster in completely dissociated junctions). The behavior observed in dissociating contacts most probably corresponds to an effective diffusion behavior, including multiple disengagement steps at the membrane. This confirms that the inhibition of cadherin dynamics in mature junctions is indeed due to endocytosis inhibition, and not to the blockade of disengagement.

Method: Dissociating junctions were obtained through a partial disruption of mature junctions, via calcium depletion. Cells were incubated in DMEM with 4 mM EDTA for 30 to 60 min, until they began to round up. FRAP was performed after a 15 min incubation in HBSS supplemented with 100 μM calcium, which prevented further dissociation; in some experiments dynasore (60 μM) was added to this incubation medium to test the effect of endocytosis inhibition.

Dynasore and MiTMAB Effects in MCF7 Cells. Dynasore and MiTMAB are efficient in inhibiting endocytosis in MCF7 cells, as shown by FM4–64 vesicles counting (the weak signal in MCF7 cells did not allow to perform a reliable co-localization counting) (see Table S3).

It has previously been reported that E-cadherin endocytosis occurred via clathrin-dependant mechanisms in MDCK cells, but via clathrin-independent mechanisms in (isolated) MCF7 cells (11). Because dynasore and MiTMAB act on dynamins (which play a key role in clathrin-dependant endocytosis), they might not inhibit, or only partially, E-cadherin-GFP FRAP recovery in MCF7 cells, in contrast to the total inhibition seen in MDCK cells. Indeed, the inhibition of E-cadherin dynamics in MCF7 cells was only partial (Fig. S8). Two different behaviors were observed: either the recovery was close to the one observed in untreated cells (blue: the membrane residence time is 40 s, similar to the one of 50 s observed in untreated cells; the mobile fraction is slightly weaker, 70% vs. 95% in the untreated case); either the recovery is inhibited (red). The precise reason for the existence of two different behaviours is not known (e.g., MCF7 cells might use either only clathrin-independent mechanisms, either a combination of both clathrin-dependent and independent mechanisms, depending on factors like the E-cadherin membrane concentration). We obtained very similar results in this cell line with MiTMAB.

Possible Implications for the Different E-Cadherin Kinetics in MCF7 and MDCK Cells. Although many actors (myosins, actin) are implicated, it is tempting to speculate that the different residence times of E-cadherin at MCF7 and MDCK junctions could be directly linked to a different stabilities of their adherens junctions. A videomicroscopy analysis showed that MCF7 and MDCK adherens junctions underwent small position fluctuations of typical amplitude 0.1 μm in 30 s, with faster oscillations for MCF7 than for MDCK (period mean is respectively 165 $\pm$ 13 and 240 $\pm$ 45 s, $n = 33$ and 35, Fig. S9). Therefore, the cell line with the shortest E-cadherin residence time in junctions has also the fastest junction fluctuation oscillations. Further studies with perturbative approached will be needed to see if E-cadherin dynamics is indeed directly coupled to the stability of junctions and to the maintenance of mechanical epithelial homeostasis.

1. Coscoy S, et al. (2002) Molecular analysis of microscopic ezrin dynamics by two-photon FRAP. *Proc Natl Acad Sci USA* 99:12813–12818.

2. Sprague BL, Pego RL, Stavreva DA, McNally JG (2004) Analysis of binding reactions by fluorescence recovery after photobleaching. *Biophys J* 86:3473–3495.

3. Iino R, Koyama I, Kusumi A (2001) Single molecule imaging of green fluorescent proteins in living cells: E-cadherin forms oligomers on the free cell surface. *Biophys J* 80:2667–2677.
4. Kusumi A, Sako Y, Yamamoto M (1993) Confined lateral diffusion of membrane receptors as studied by single particle tracking (nanovid microscopy). *Effects of calcium-induced differentiation in cultured epithelial cells* Biophys J 65:2021–2040.
5. Macia E, et al. (2006) *Dynasore, a cell-permeable inhibitor of dynamin* Dev Cell 10:839–850.
6. Quan A, et al. (2007) Myristyl trimethyl ammonium bromide and octadecyl trimethyl ammonium bromide are surface-active small molecule dynamin inhibitors that block endocytosis mediated by dynamin I or dynamin II. *Mol Pharmacol* 72:1425–1439.
7. Waharte F, Brown CM, Coscoy S, Coudrier E, Amblard F (2005) A two-photon FRAP analysis of the cytoskeleton dynamics in the microvilli of intestinal cells. *Biophys J* 88:1467–1478.
8. Adams CL, Chen YT, Smith SJ, Nelson WJ (1998) Mechanisms of epithelial cell-cell adhesion and cell compaction revealed by high-resolution tracking of E-cadherin-green fluorescent protein. *J Cell Biol* 142:1105–1119.
9. Causeret M, Taulet N, Comunale F, Favard C, Gauthier-Rouviere C (2005) N-cadherin association with lipid rafts regulates its dynamic assembly at cell-cell junctions in C2C12 myoblasts. *Mol Biol Cell* 16:2168–2180.
10. Sako Y, Nagafuchi A, Tsukita S, Takeichi M, Kusumi A (1998) Cytoplasmic regulation of the movement of E-cadherin on the free cell surface as studied by optical tweezers and single particle tracking: Corralling and tethering by the membrane skeleton. *J Cell Biol* 140:1227–1240.
11. Paterson AD, Parton RG, Ferguson C, Stow JL, Yap AS (2003) Characterization of E-cadherin endocytosis in isolated MCF-7 and chinese hamster ovary cells: the initial fate of unbound E-cadherin. *J Biol Chem* 278:21050–21057.

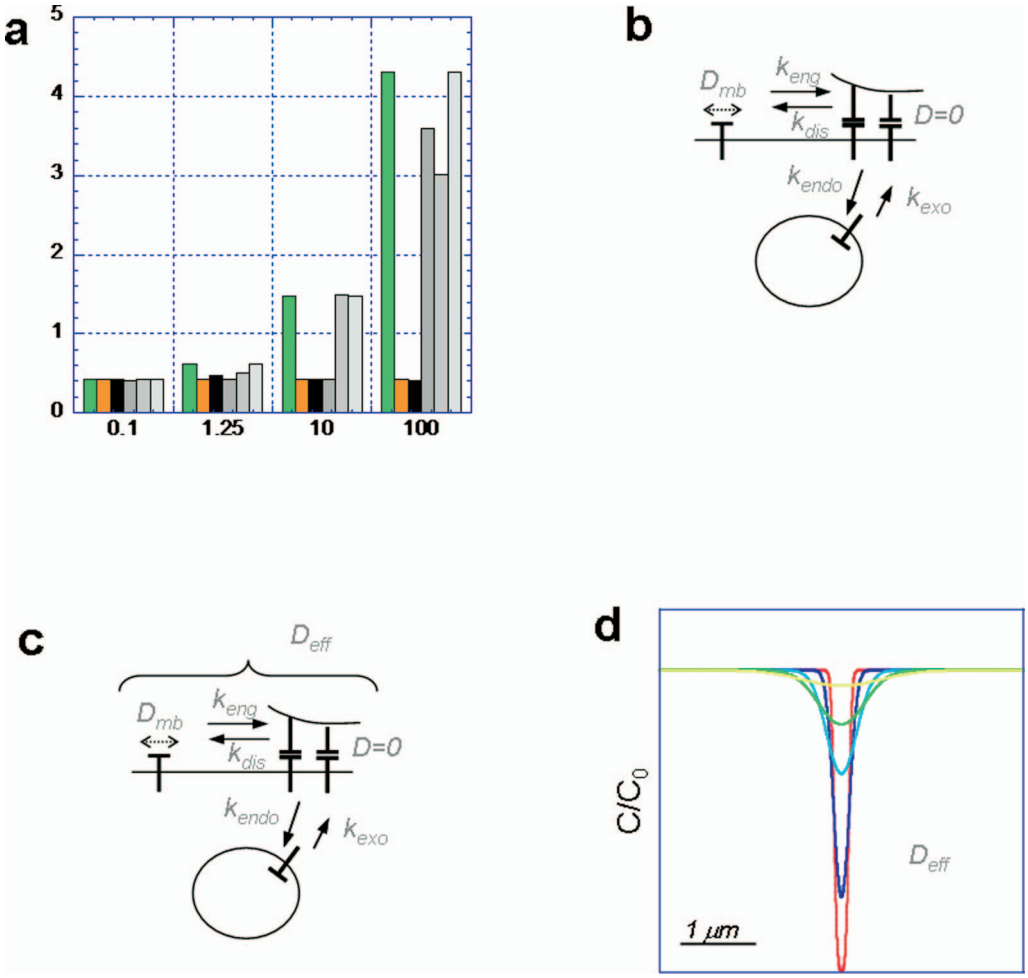

Fig. S1. Broadening of fluorescence profiles when diffusion is combined with exchange. (*a*) Width σ of Gaussian fits made for fluorescence profiles as a function of the elapsed time. Fits were made over the region that surrounds photobleached point (3 $\sigma_{PSF} = 1.5$ μm). Different processes were considered: (*i*) diffusion only (green) characterized by a diffusion time $\tau_d = \sigma_{PSF}^2/4D$ where σ_{PSF} is the transversal size of the point spread function, (*ii*) first-order reaction-limited exchange only (orange) characterized by an exchange time τ_c (k_{off}^{-1}), or (*iii*) combinations in equal amounts of two independent pools undergoing diffusion or exchange. In the latter case, various times scales configurations were considered: $\tau_c/\tau_d = 100$, 10, 1 and 0.1 (respectively black, successive greys, white). Here $\tau_d = 1.25$ s, corresponding to $D = 5 \times 10^{-2}$ $\mu m^2 \cdot s^{-1}$ for 2D diffusion. (*b*) Schematic representation of the general situation involving exchanges both at membrane with an immobile state and with cytosolic vesicles through endocytosis. (*c* and *d*) Case of fast membrane exchanges. Under the simplifying hypothesis that of a single diffusive membrane pool with an ''effective'' diffusion coefficient $D_{eff} < D_{mb[infi]}$. (*c*) The width of the Gaussian fits (*d*) behaves as for simple diffusion (green bars in a).

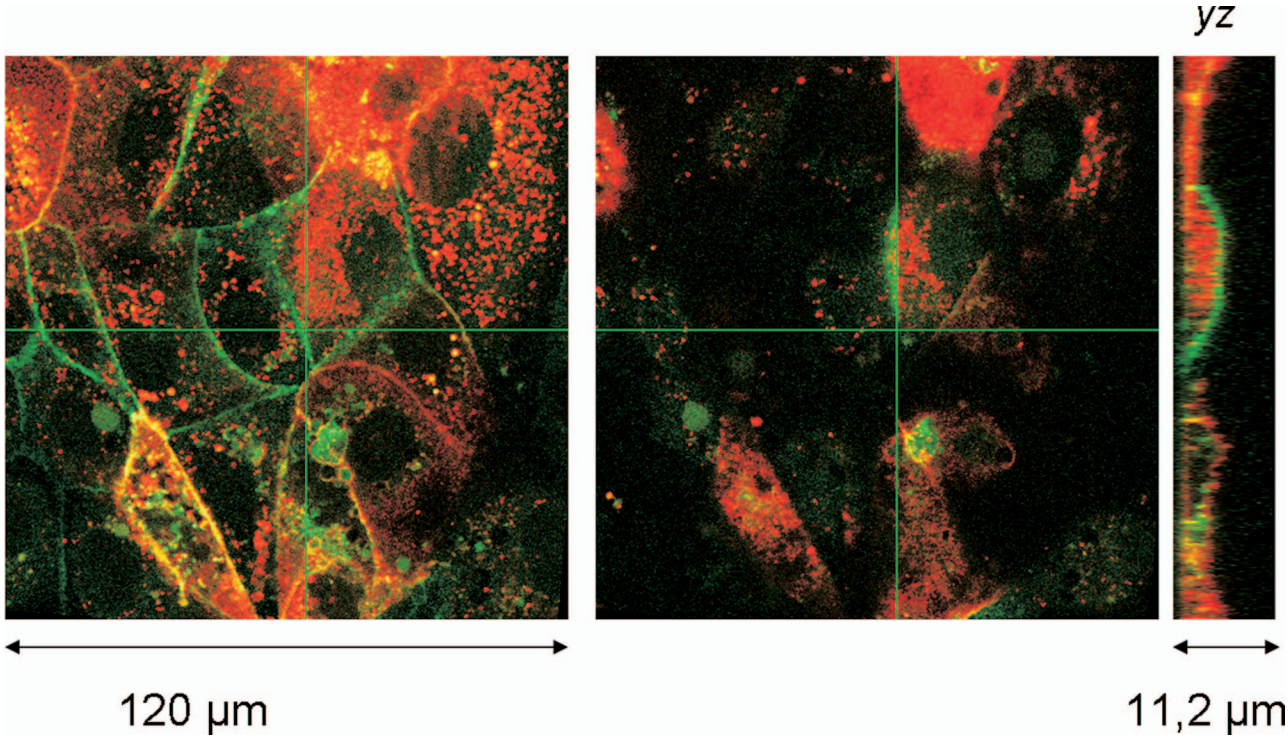

Fig. S2. *z* distribution of E-cadherin-GFP. MDCK cells transiently expressing RFP-CAAX as a membrane marker (red) and labeled with anti-E-cadherin antibody (green) were imaged on a confocal microscope (Leica SP2 AOBS). Two *z*-planes ($\Delta z = 2\ \mu$m) are shown, as well as an *y-z* section (section along the vertical green lines in *xy* images). The typical width of the E-cadherin stripe at *adherens* junctions is estimated from these *y–z* images.

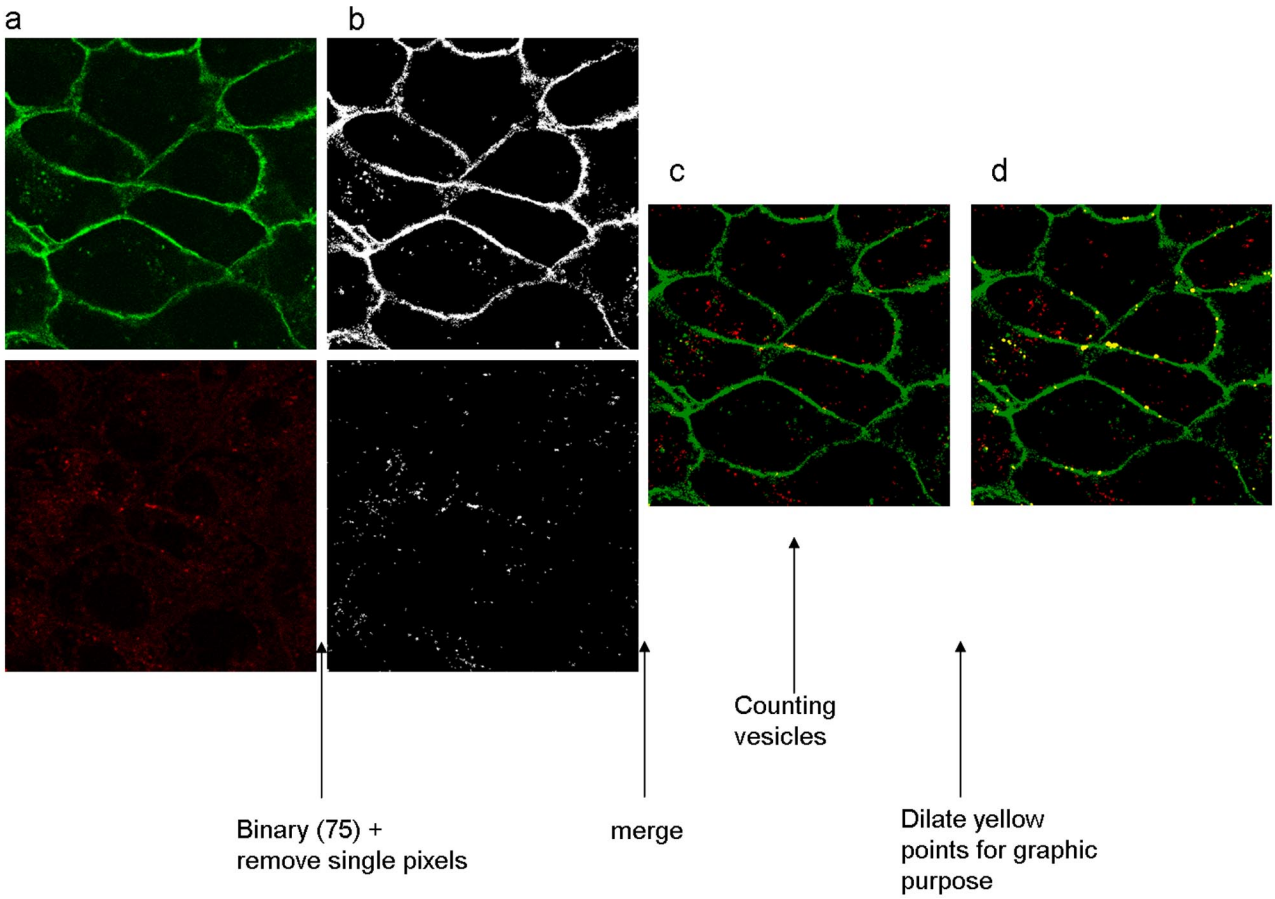

Fig. S3. Image processing of co-localization data. Colocalization images of FM4–64 (red) and E-cadherin-GFP (green) in MDCK cells (*a*). To count newly formed vesicles, 8 bits images were first binarized using a common threshold (75/256 and 90/256 for the green and the red channel) (*b*), single pixels were removed and images were merged (*c*) at this step, cytosolic vesicles were manually counted to exclude positive points at the plasma membrane (*cf.* Table 1 of the article). To improve the visualization vesicles on down-scaled images (Fig. 3), yellow points have been slightly enlarged (*d*).

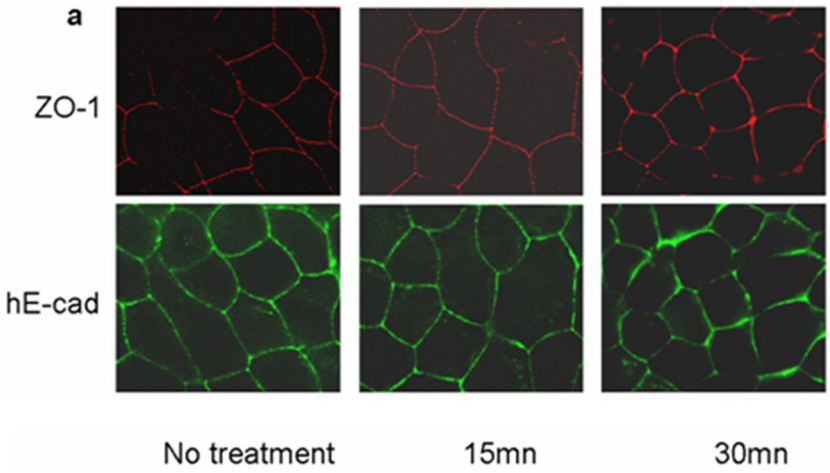

Fig. S4. Morphology of MDCK cells after dynasore treatment. Immunolabeling of ZO-1 (red) and human E-cadherin (green) on confluent MDCK cells, before (first column), or after a 15 min (second column), or a 30 min (third column) incubation with 60 μM dynasore.

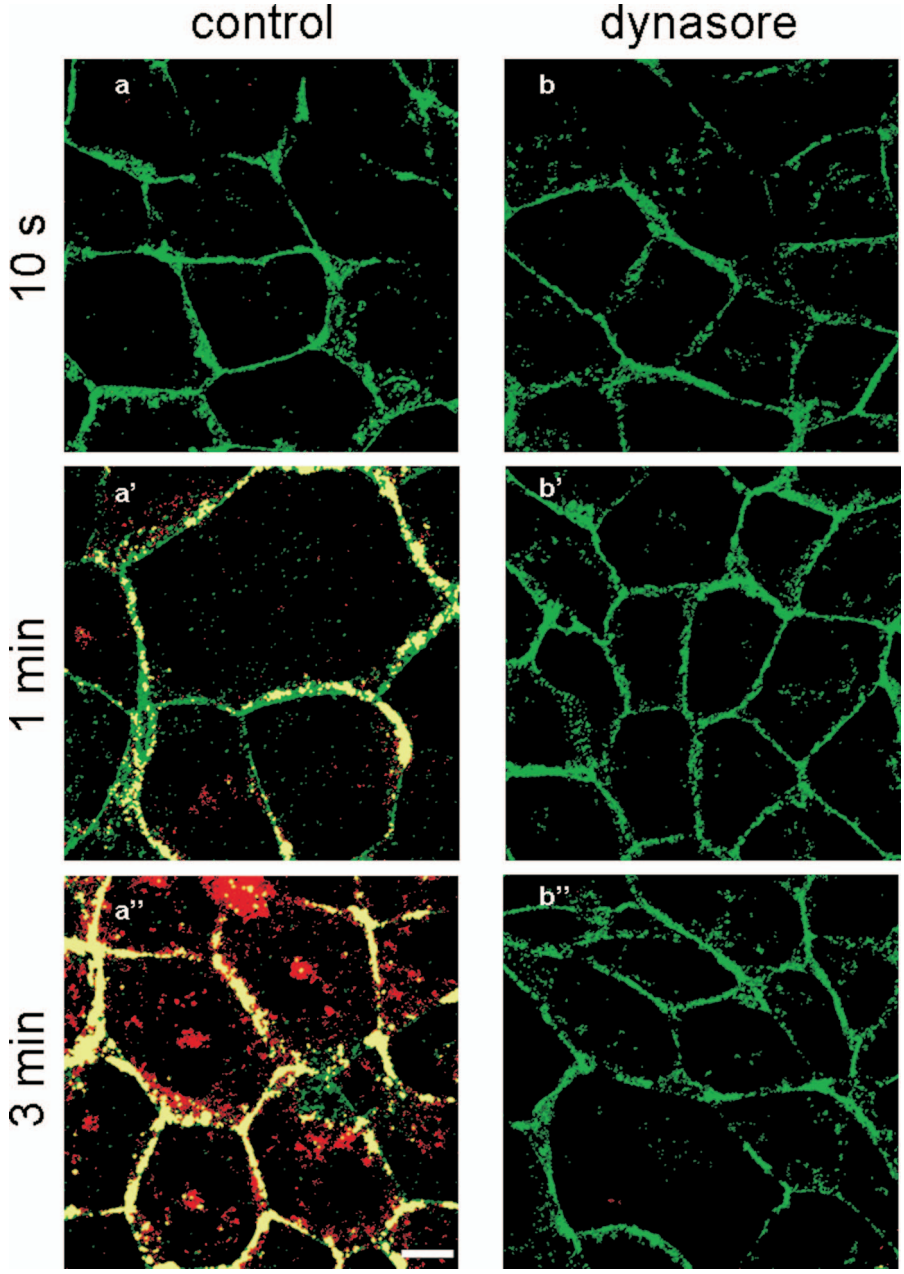

Fig. S5. newly formed E-cadherin vesicles in wild-type MDCK. After treatment with control medium (*a*, *a'*, *a''*) or dynasore 60 μM (*b*, *b'*, *b''*) MDCK E-cadherin-GFP cells were incubated with FM 4–64 5 μg/ml for the indicated times to visualize newly formed endocytosis vesicles (appears in red). Cells were then fixed and E-cadherin stained by immuno-labeling (green). Merge image of the green and red staining are shown, and colocalisation appears in yellow.

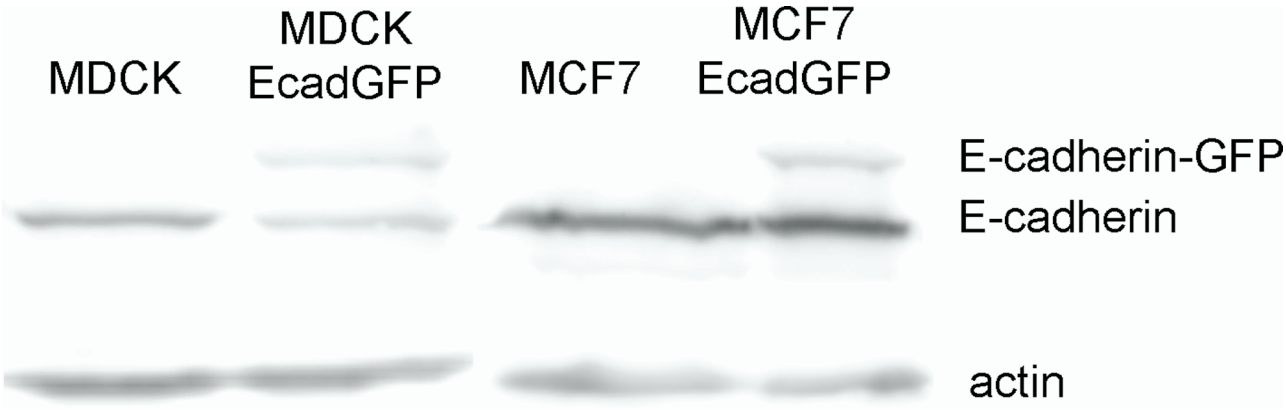

Fig. S6. Western blots for E-cadherin quantification in transfected vs. wild-type MDCK and MCF7 cells. Total cell extracts were obtained from lysates of confluent monolayers of WT MCF7, MCF7 Ecadh-GFP, WT MDCK and MDCK Ecadh-GFP. We compared the levels of E-cadherin, normalized by inputs levels as measured by actin quantity, in MDCK vs. MDCK-E-cadherin-GFP, and in MCF7 vs. MCF7-E-cadherin-GFP.

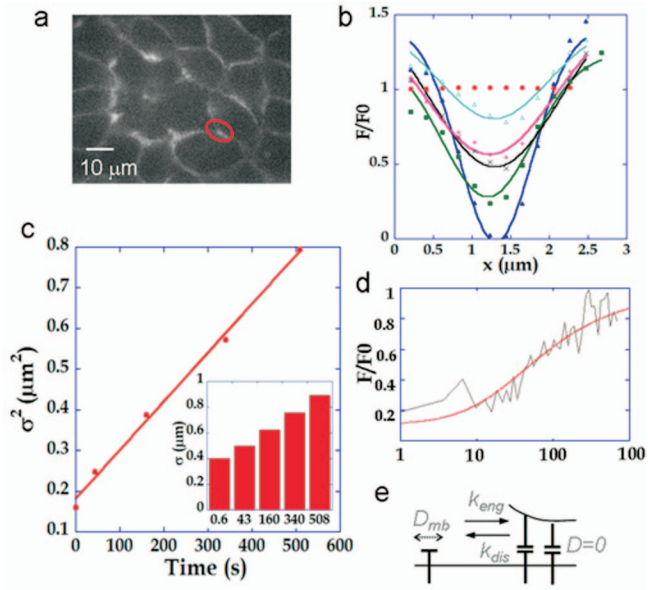

Fig. S7. Membrane diffusion is present in dissociating junctions between MDCK cells. (*a*) Typical image of cells with dissociating junctions at intermediate Ca^{2+} levels in the presence of 4 mM EDTA, and with dynasore. FRAP was monitored in ''almost dissociated'' junctions (red ellipse). (*b*) Fluorescence profiles before bleaching (red o), or 0.6 s (blue Δ), 43 s (green □), 160 s (black x), 340 s (pink +) or 510 s (cyan Δ) after bleaching. (*c*) The width σ of the Gaussian fits of the experimental fluorescence profiles (solid lines in *b*) increases with time (*c Lower Right Inset*). σ^2 is linear with time ($\sigma^2 = 0.1811 + 0.0012 \times t$, $R = 0.998$). (*d*) The recovery curve (gray) is best fitted by a diffusion process (red), with $D = 0.0025\ \mu m^2 \cdot s^{-1}$. (e) Model of effective diffusion for E-cadherin exchanging between a diffusive state and an immobile engaged state.

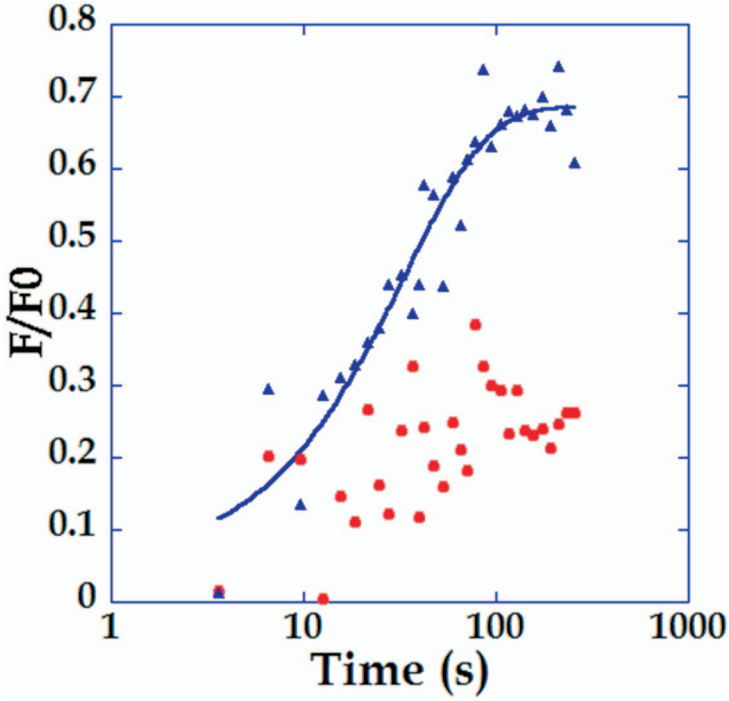

Fig. S8. FRAP curves in MCF7-E-cadherin-GFP cells treated with dynasore. With respect to FRAP experiments, MCF7 cells behave differently. In some cells (40%), fluorescence recovery was inhibited (red), but not in the remaining cells (blue) where the was similar to untreated cells, with an exponential relaxation (residence time $\approx$ 40 s, mobile fraction $\approx$ 70%). (Mean of $n = 13$ for the non-relaxing curve, $n = 14$ for the relaxing one.)

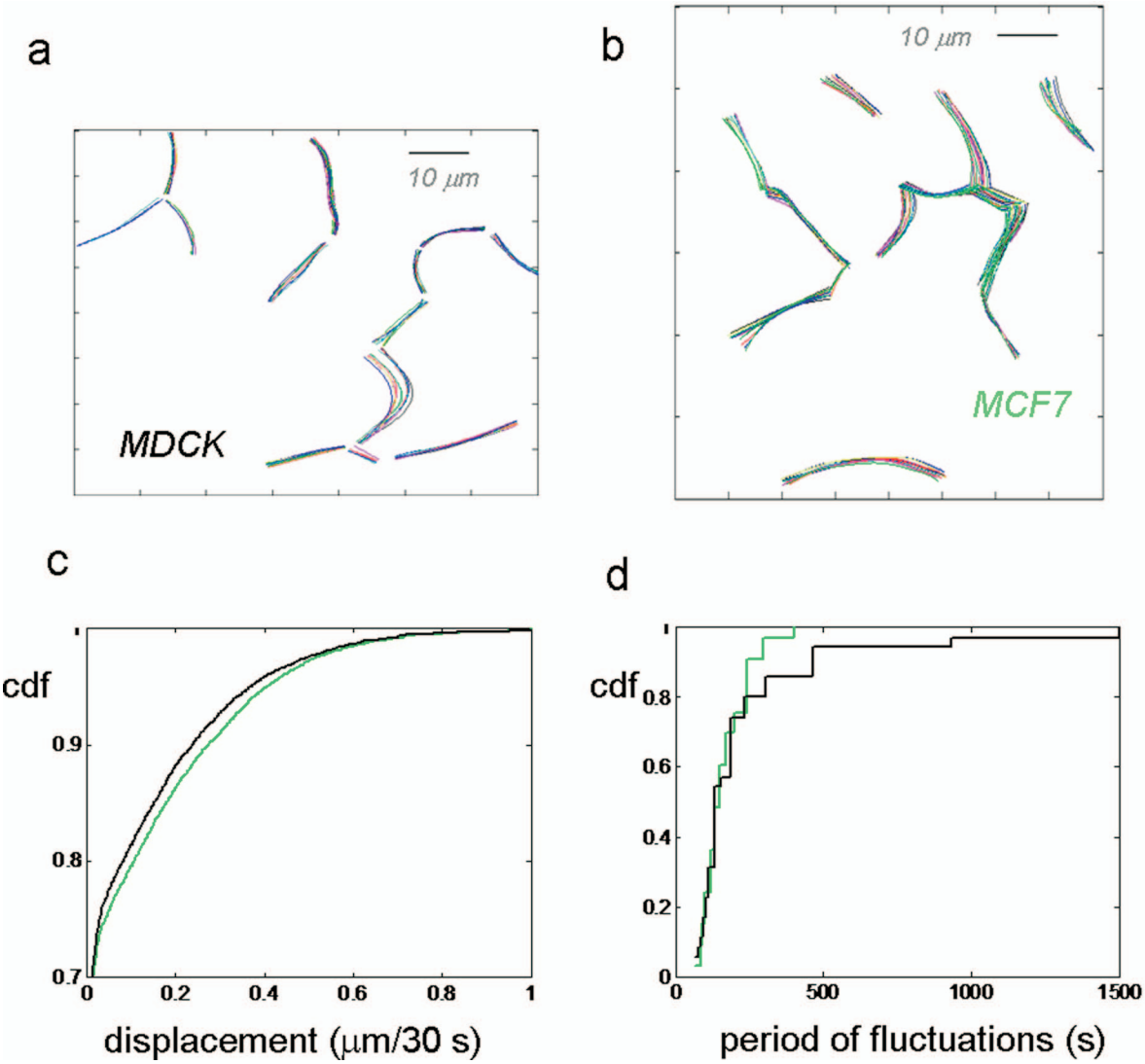

Fig. S9. Junctions move differently in MDCK and MCF7 cells. (*a*) Using videomicroscopy film of MDCK and MCF7 cells expressing E-cadherin-GFP (with a typical image rate of 1/30 s over 30 min), junctions were manually tracked (*a* and *b*). The amplitude of perpendicular displacements over 30 s for all junctions is shown as a cumulated distribution function (*c*). Junctions were seen to oscillate about stable average positions, and their motion individually reverted many time during the observation period. To assess typical period of these oscillations, the distribution of time interval between successive direction reversals was measured and is shown as a cumulated distribution function (*d*).

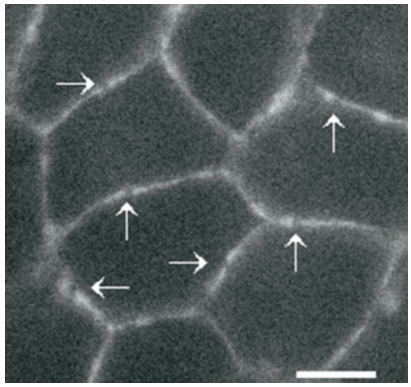

Movie S1. MDCK. Two-photon FRAP on MDCK junctions expressing E-cadherin-GFP. Images of a FRAP experiment (each image is the projection of 14 *z*-planes, see movie S2). Photobleached regions are indicated by arrows. The total duration is 30 min. Scale bar: 10 μm.

Movie S1 (MOV)

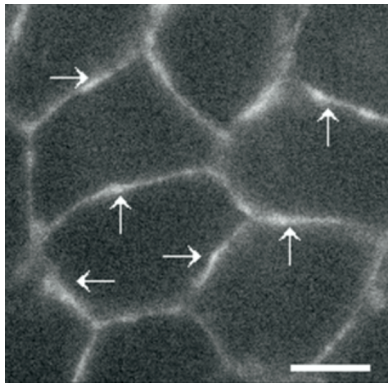

Movie S2. MDCK before. *z*-stack before photobleaching. $\Delta z = 0.3$ μm.

Movie S2 (MOV)

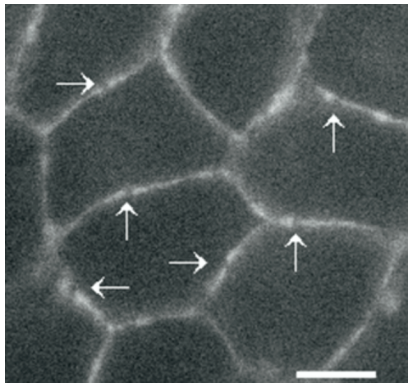

Movie S3. MDCK after. *z*-stack immediately after photobleaching. $\Delta z = 0.3\ \mu m$.

Movie S3 (MOV)

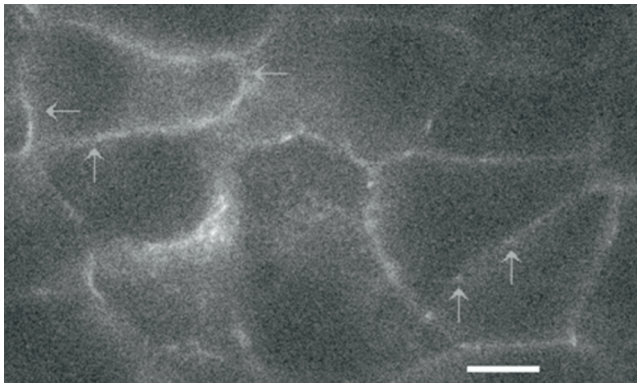

Movie S4. MCF7. Two-photon FRAP on MCF7 junctions expressing E-cadherin-GFP. Images of a FRAP experiment (projection of 12 *z* planes). Photobleached regions are indicated by arrows. The total duration is 4 min. Scale bar: 10 μm.

Movie S4 (MOV)

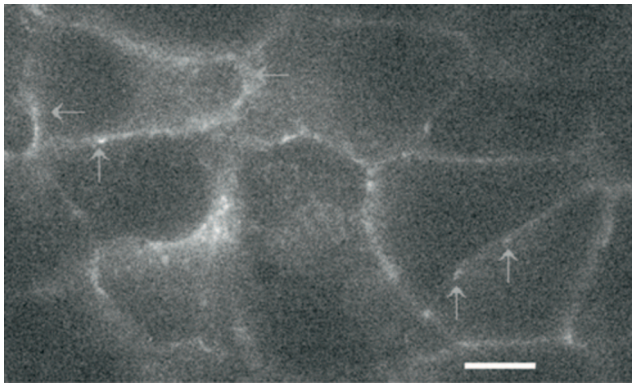

Movie S5. MCF7 before. *z*-stack (wider area) before photobleaching. $\Delta z = 0.3\ \mu m$.

Movie S5 (MOV)

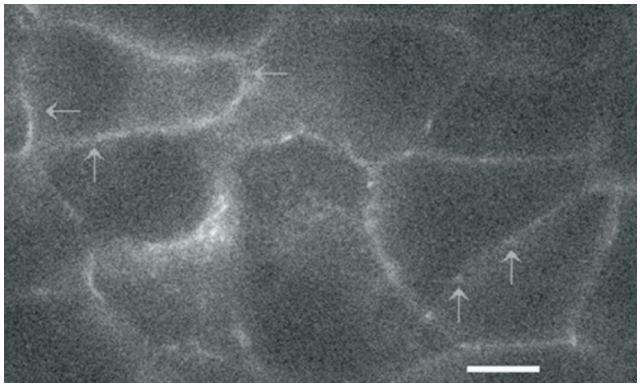

Movie S6. MCF7 after. *z*-stack (wider area) immediately after photobleaching. $\Delta z = 0.3\ \mu m$.

Movie S6 (MOV)

Table S1. Vesicles counted in wild-type MDCK cells

	FM4–64 vesicles		Ecadh vesicles		Colocalization	
	Control	Dynasore	Control	Dynasore	Control	Dynasore
FM4–64 10 s	11 ± 10	0			Not detectable	
FM4–64 1 min	52 ± 26	0	148 ± 26	130 ± 20	7 ± 3%*	<1%
FM4–64 3 min	250 ± 26	0			44 ± 14%**	<1%

Table S2. Biochemical quantification of E-cadherin amounts in wild-type vs. transfected cell lines

	WT	Transfected/WT		
MCF7	100%	115%	78%	E-cadh
			22%	E-cadh-GFP
MDCK	100%	92%	58%	E-cadh
			42%	E-cadh-GFP

Table S3. Vesicles counted in MCF7 cells expressing E-cadherin-GFP

	FM 4–64 vesicles (red)			E-cadh-GFP vesicles (green)		
MCF7	Control	Dynasore	MiTMAB	Control	Dynasore	MiTMAB
FM4–64 1 min	220 ± 20	29 ± 6	44 ± 17	20 ± 4	15 ± 3	14 ± 2